NASA Technical Memorandum 106098

IN-18

157791

P. 12

Plasma Sheath Effects on Ion Collection by a Pinhole

Joel L. Herr
Sverdrup Technology, Inc.
Lewis Research Center Group
Brook Park, Ohio

and

David B. Snyder
National Aeronautics and Space Administration
Lewis Research Center
Cleveland, Ohio

NASA
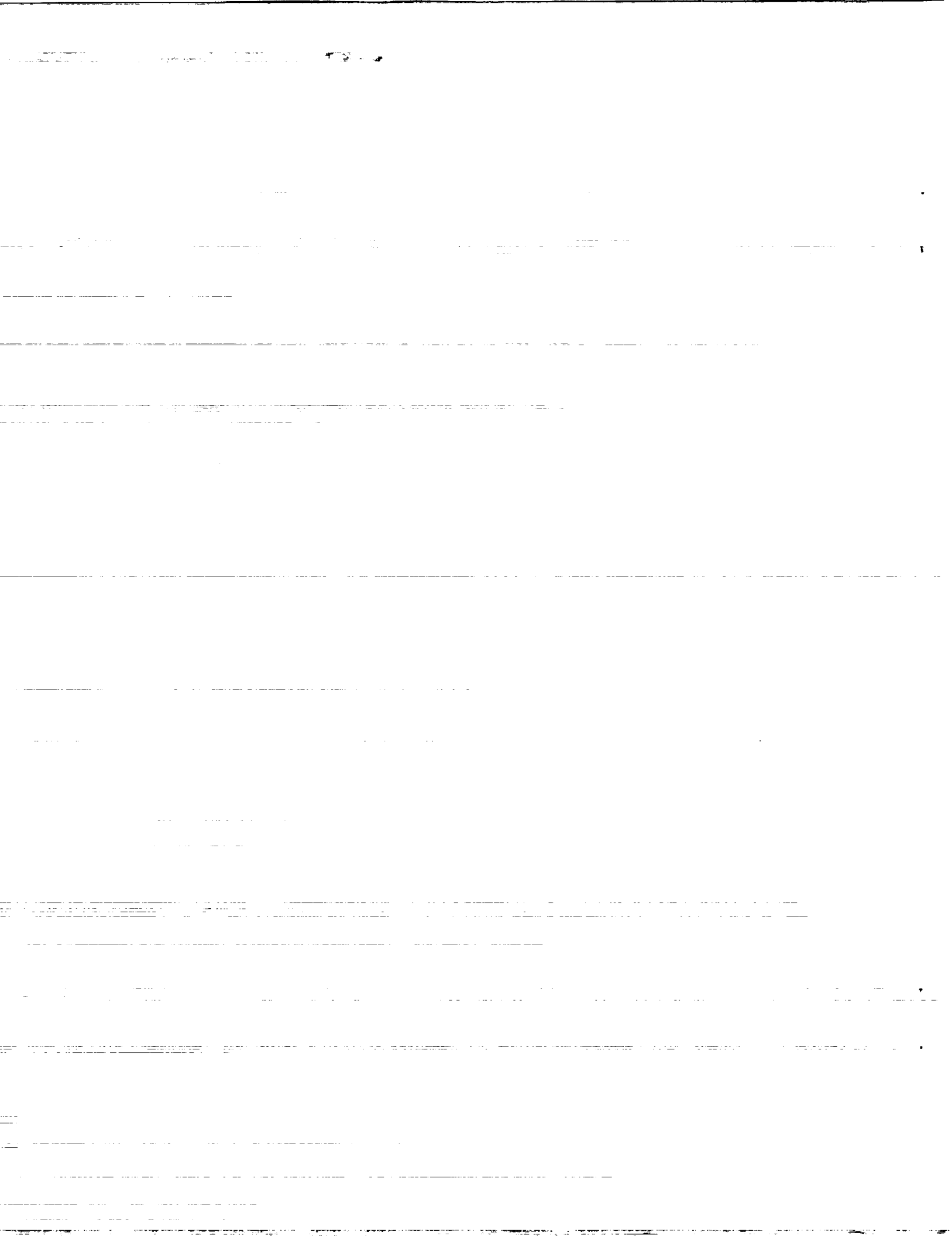
Plasma Sheath Effects on Ion Collection by a Pinhole

Joel L. Herr
Sverdrup Technology, Inc.
Lewis Research Center Group
Brook Park, Ohio 44142

David B. Snyder
National Aeronautics and Space Administration
Lewis Research Center
Cleveland, Ohio 44135

This work presents tables to assist in the evaluation of pinhole collection effects on spacecraft. These tables summarize results of a computer model which tracks particle trajectories through a simplified electric field in the plasma sheath. A technique is proposed to account for plasma sheath effects in the application of these results and scaling rules are proposed to apply the calculations to specific situations. This model is compared to ion current measurements obtained by another worker, and the agreement is very good.

INTRODUCTION

Ionospheric plasma interactions can result in spacecraft structure potentials being substantially more negative than the ambient environment[1], especially on high power spacecraft supported by high voltage solar arrays. Among other things this can result in sputtering of spacecraft surfaces by the collected ions if the potential difference is negative enough. This sputtering may become a concern in three ways: it may be a source of contamination for surfaces closer to the plasma potential; it may cause failure of grounded metal foils; and as the effective ion collection area grows structure currents and power losses will grow.

Sites of special concern are grounded metal surfaces covered with insulating dielectric films exposed to the ionospheric plasma. Even though in general these films will be protective, defects in these films caused by the manufacturing process, micrometeoroid and debris hits, or dielectric breakdown, will result in the focusing of the collected ions onto local spots of the metal. The enhanced ion collection will be significantly more than that estimated from only the ion flux to the surface and the area of the defect, possibly resulting in enhanced sputter rates.

In order to calculate the ion current to the surface a focus factor can be estimated. This focus factor is a characteristic of the geometry and conditions of and near the defect. Once it is evaluated, the current to the defect is given by the product of the ion flux and the defect area with the focus factor.

* Member AIAA

Work on problems with similar electric field geometries has been performed by various workers. These problems include electron "snapover" near pinholes[2-6], and focusing onto dielectric surfaces[7]. These studies include physical processes that are not necessary for the ion collection analysis, though generally the final results are similar.

The work presented here is an extension of an effort[8] to develop a simple quantitative model to estimate the ion current collection to holes in spacecraft insulating surfaces in ionospheric plasma. This work incorporates a technique to estimate the size of the plasma sheath, rather than treating the sheath as a free parameter. Also suggestions are made as to how the parameters can be scaled to permit application of a relatively small data set to a wide range of physical situations. Results of focus factor estimates are tabulated, permitting interpolation to estimate current collection. In addition, calculated results are compared to some experimental observations.

MODEL

Original Model

The approach taken in this model is to solve Laplace's equation for a pinhole geometry in a region representative of a plasma sheath, then track ion trajectories through the resulting potential field. The fields and trajectories are determined in two dimensions with cylindrical symmetry assumed about the axis of the hole, as shown in Fig. 1. However velocities are tracked in three dimensions to permit accommodation of angular momentum considerations. The focus factor for a particular incident velocity vector is the ratio of the area of initial positions from which ions will hit in the hole to the area of the hole. Ion current to the hole can then be calculated from the product of the hole

area, the focus factor and the incident ion current density for the sheath edge.

The calculation region used is representative of the plasma sheath. The electric fields near the hole are calculated by solving Laplace's equation rather than Poisson's equation. This is appropriate when the bias is large compared to the plasma temperatures, and the density of the collected ions does not get too high. This is usually true since the ions accelerate as they leave the plasma sheath edge. Also, while ion trajectories may be affected by increased ion density due to the focusing, in practice the ions tend to hit near the center of the conductor, and deflecting the trajectories outward slightly will not effect the observed ion current.

The boundary conditions are simplified by assuming the upper boundary of the rectangular calculation space is at zero potential. This represents the upper boundary of the plasma sheath, and it is assumed to be parallel to the surface. The lower boundary is divided into two regions, a central hole region at the biased potential, and a dielectric region at zero potential. The bias potential represents the electric potential difference between the ambient plasma and the spacecraft ground. Since dielectrics generally charge to a small negative potential, comparable to the electron temperature, and the hole region is metal, this assumption is reasonable as long as the bias is much larger than the potential difference attained between the dielectric and the plasma. The central and outer boundaries are set so that the radial electric field is zero. At the center this is true by symmetry. It is also true at the outer boundary if it is far enough away.

This simplified field approach ignores the electric field structure at the hole dielectric edge and the depth of the hole, which should have only short range effects. In this case short range means that if the particle gets close enough to experience them, it will probably hit within the hole. But the issue may be important for very small defects where the insulator conductivity may result in an effective hole size substantially larger than the defect. It also ignores the electric field between the dielectric and the plasma due to the thermal plasma sheath. However, this should be negligible, and the assumption reduces the dimension of the model's parameter space.

Secondary electron emission effects are neglected. 'Snapover' on the insulation is not important in this case since the electric field on the insulators prevents the secondaries from escaping.
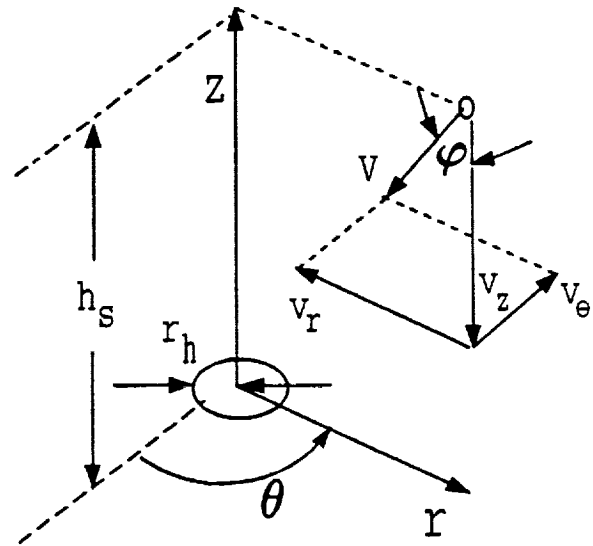

Figure 1: Calculation Region

On the conductor, secondary yields may be on the order of 10%, but this is small compared to uncertainties in the plasma parameters and may be neglected for engineering level calculations, or added explicitly on a case by case basis.

The particle velocity is tracked in three dimensions. The potential field around the hole has cylindrical symmetry so the position angular coordinate of the ion trajectory is not important. However the angular velocity component plays a significant role since this component is needed to conserve angular momentum about the axis of symmetry. Angular effects are accounted for by calculating the displacement over the time interval, then rotating the coordinate system to find the new values for r, z, v_r, v_z and v_θ.

The focus factor is the ratio of the area where incident particles will hit inside the hole, to the area of the hole. For cylindrical symmetry this is the ratio, r_i^2/r_h^2, where r_i is the maximum incident radius that ions are collected from, and r_h is the radius of the hole. At large angles of incidence, this expression may have to be corrected to account for the fact that there can be a minimum radius, inside which incident ions are not collected. This definition is convenient for determining ion currents, and sputter rates as contamination sources.
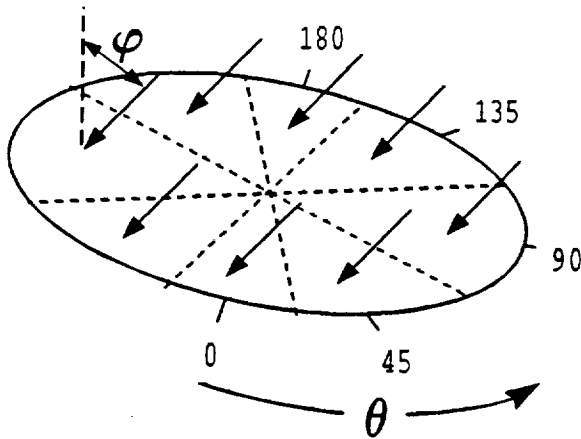
2

Figure 2: Illustration of incident velocity variation for the different sectors of the calculation.

However, this is an underestimate for local damage rates since almost all the collected particles hit inside the radius, $r_h/2$.

Even though the electric field in this problem has cylindrical symmetry, this symmetry is destroyed by an incoming flux of particles with a non-zero angle of incidence, φ. In this case the focus factor depends on the angle coordinate, θ. In order to take into account the θ dependence, the 360 degree range for values of θ are divided into a number of sectors as illustrated in Fig. 2, each with a representative value for θ, and a representative value of the focus factor is found for that sector. An even number of sectors is used, including ones centered on 0 and 180 degrees. In practice 45 degree sectors are used. However, because of the symmetry of the problem only half the other sectors need to be calculated, either $0 < \theta < 180$ degrees or $180 < \theta < 360$ degrees. Those sectors at zero and 180 degrees are given a weighting of one while the others are given a weighting of two to account for the missing but opposite sectors. The net focus factor is the average of the sector focus factors.

The effect of an ion temperature can be addressed by adding incremental velocities representative of a three-dimensional Maxwell velocity distribution to an incident velocity. To calculate a focus factor for a given incident angle and temperature, the three dimensional initial velocity

distribution is broken into a cartesian grid. A representative velocity vector is chosen at the center of each grid element and a focus factor is calculated for each grid element. Since only half the elements need be calculated because those with a velocity element in the $+\hat{\theta}$ have the same focus factor as the corresponding element in the $-\hat{\theta}$ direction, division of the three dimensional velocity space into approximately 3000 elements (18x18x9) yields a reasonable simulation. Each grid element is assigned a composite velocity vector representative of its position and weighted first by the probability of the particle having a velocity near the tested value, and secondly by which θ sector the computation is being performed in.

Plasma Sheath

Since in the present model the plasma sheath region is equated with the calculation space, it is critical to be able to estimate the thickness of the sheath. This is accomplished by comparing the Laplacian solution with no upper boundary to the charge density of the influx of ions from the plasma. The location of the sheath edge, h_s can be estimated by determining where the second partial derivative of the potential, ϕ, with respect to height above the hole is equal to the ion charge density flowing into the sheath. This condition is expressed by,

$$\left. \frac{\partial^2 \phi}{\partial h^2} \right|_{h_s} = \frac{\rho(h_s)}{\varepsilon_0}.$$

This is not a rigorous technique but finds the place where the geometric distortion of the field is comparable to that due to the space charge. If the magnitude of each of the two terms of the Laplacian operator for cylindrical symmetry is much larger than the charge density term, the potential field is primarily influenced by the boundary conditions, and Laplace's equation is appropriate. But when the terms get as small as the charge density term, Poisson's equation clearly should be used. We avoid the problem by assuming this condition indicates the edge of the plasma sheath. This condition is used to estimate the sheath edge location.
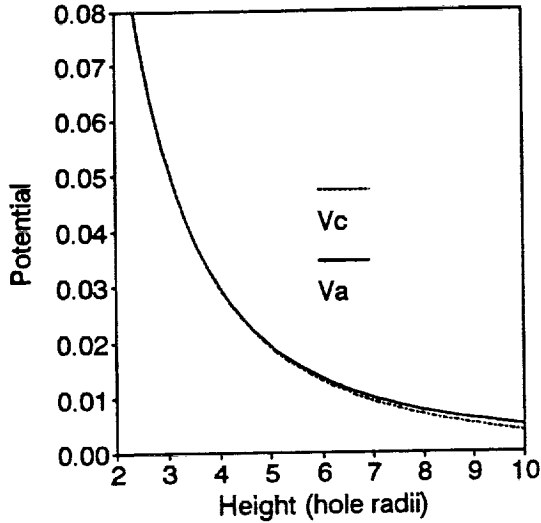
3

Figure 3: Comparison between an analytical expression, $V_a = (1 - h/\sqrt{r_h^2 + h^2})$, for the electric potential above a pinhole and a calculated finite difference solution, V_c, to Laplace's equation.

In order to do this comparison, an analytical expression was found for the potential along the axis above the hole. A technique was used which has occasionally, but not reliably, found analytical solutions to Laplace's equation. The potential at a point is assumed to be the average of defined surface potentials weighted by the solid angle covered. The result is then checked against Laplace's equation to see if it is correct. The average angular potential, V_a, seen at a height, h, above the center ($r=0$) of the biased hole is obtained from,

$$V_a(h) = \int_0^{arctan(r_h/h)} \phi(h{=}0, r) \sin(\theta) \, d\theta$$

$$= V_0 \left(1 - \frac{h}{\sqrt{r_h^2 + h^2}} \right),$$

where $\phi(h{=}0, r) = V_0$ for $r < r_h$ and $\phi(h{=}0, r) = 0$ for $r > r_h$. Since this expression was not found rigorously, it is compared to a solution found by finite differencing in Fig. 3. The maximum difference between the two is about 0.001 times the bias voltage within 10 hole radii on the conductor. It can be seen that the agreement is excellent until the finite difference solution is forced to zero at the upper boundary of the calculation space.

The value obtained above should be compared with the Debye length for the plasma. The Debye length gives an idea of the plasma sheath associated

with the surface, and if the surface's thermal sheath is thicker than the sheath associated with the hole, the assumptions made in this model are not appropriate.

Scaling Rules

The pinhole ion collection problem has six parameters; hole radius and bias, plasma speed and temperature, the angle that the ions' velocity vector makes with the axis of symmetry, and the plasma sheath thickness. However, it is apparent that a number of interesting parameters are interrelated so that results are reported in terms of only four parameters: normalized plasma ram energy and incident angle, normalized ion temperature, and normalized sheath thickness. These simplifications are reasonable if two issues are demonstrated, (1) the electric field depends only on the grid chosen and can be scaled with the magnitude of the applied bias and the hole radius, and (2) the trajectory of the particle within the grid depends only on the scaled electric field, the incident kinetic energy to bias ratio, and the velocity direction. The following discussion, while not rigorous, suggests that this is indeed the case.

The electric field in the calculation space is obtained by setting certain boundary conditions, and satisfying Laplace's equation. First consider only the applied bias. If $\nabla^2\phi(r, z) = 0$ then $\nabla^2 V_0\phi(r, z) = 0$ is also satisfied, where V_0 is a constant adjusted to match the voltage difference. The electric field is given by $V_0\nabla\phi^*(r, z)$ where $\phi^*(r, z)$ is the potential field that matches the boundary conditions when the bias is one.

There are three distance scales in the definition of the problem, the radius of the hole, the height of the calculation space, i.e. the plasma sheath thickness, and the width of the calculation space. Ideally the width of the calculation space would be infinite, and in practice it should be large enough that it does not effect the calculation significantly. This leaves only two distance scales, the sheath thickness in the $\hat{z}$ direction and the hole radius in the $\hat{r}$ direction.

In practice the potential field is found for positions on a grid using a finite difference equation. For cylindrical symmetry, this comes from,

$$\nabla^2\phi = \frac{1}{r}\frac{\partial}{\partial r}\left(r\frac{\partial\phi}{\partial r} \right) + \frac{\partial^2\phi}{\partial z^2}.$$

4

At the grid position $(i\Delta r, j\Delta z)$ the finite difference equation becomes,

$$\phi_{i,j} = \frac{a^2}{2(a^2+1)}\left[\frac{\left(i+\frac{1}{2}\right)\phi_{i+1,j} + \left(i-\frac{1}{2}\right)\phi_{i-1,j}}{i} + \frac{\phi_{i,j+1} + \phi_{i,j-1}}{a^2}\right],$$

where $a = \Delta z/\Delta r$. Note that the grid separation drops out. As long as the grid is cartesian the potential field depends only on the boundary conditions and the relative grid spacing. So as long as the width of the grid range is enough to be effectively infinite, the potential field, which depends only on the boundary conditions, depends only on the plasma sheath thickness height and hole radius ratio, for the relative grid size, and the bias potential.

It is the intention here to show that the electric field can be scaled to the grid size or the hole radius. An electric field is obtained from the potential grid using equations like,

$$E_r(i\Delta r, j\Delta z) = -V_0 \frac{\phi_{i+1,j}^* - \phi_{i-1,j}^*}{2\Delta r}.$$

Note that for a hole radius of $r_h = (l+\frac{1}{2})\Delta r$, a 'grid' electric field, $\vec{E}^*(i,j)$, relative to the hole size can be defined as,

$$E_r^*(i,j) \equiv \frac{r_h E_r(i\Delta r, j\Delta z)}{V_0}$$

$$= -\left(l+\frac{1}{2}\right)\left(\frac{\phi_{i+1,j}^* - \phi_{i-1,j}^*}{2}\right).$$

Similarly $E_z^*(i,j)$ can be obtained. The scaled electric field, $(V_0/r_h)\vec{E}^*(i,j)$, is then used in the equations of motion for the electric field.

Now the motion within the grid is examined assuming that the electric field can be scaled by $\vec{E}(r,h) = V_0\vec{E}^*(r/r_h, h/r_h)/r_h$. The model uses the two equations of motion:

$$\vec{v}(\delta t) = \vec{v}_0 + \vec{a}\delta t,$$

$$\vec{r}(\delta t) = \vec{r}_0 + \vec{v}_0\delta t + \frac{1}{2}\vec{a}\delta t^2,$$

where $\vec{a}$ is the acceleration is given by $q\vec{E}(r,h)/m$ and δt is a time interval to increment the calculation. In the limit that δt goes to zero, this will converge on the correct trajectory, and will give good results when $(\vec{r}(\delta t) - \vec{r}_0) \cdot \nabla\vec{E}$ is very

small compared to $\vec{E}$. But this time interval can be chosen so that $\delta t = \delta x/|\vec{v}_0|$, where δx is a distance interval along the particle path. Substituting the scaled electric field above, the kinetic energy, $K = \frac{1}{2}m|\vec{v}|^2$, and scaling to the hole radius distance scale, r_h produces the following two equations of motion:

$$\frac{\vec{v}(\delta t)}{r_h} = \frac{|\vec{v}_0|}{r_h}\left(\frac{\vec{v}_0}{|\vec{v}_0|} + \frac{qV_0\delta x}{2Kr_h}\vec{E}^*\left(\frac{r}{r_h}, \frac{h}{r_h}\right)\right),$$

$$\frac{\vec{r}(\delta t)}{r_h} = \frac{\vec{r}_0}{r_h} + \frac{\vec{v}_0\delta x}{|\vec{v}_0|r_h} + \frac{qV_0\delta x^2}{4Kr_h^2}\vec{E}^*\left(\frac{r}{r_h}, \frac{h}{r_h}\right).$$

The scaled trajectory, obtained from the position equation depends only on the direction of the velocity vector, $\vec{v}_0/|\vec{v}_0|$, the energy ratio, qV_0/K, and the scaled electric field $\vec{E}^*(r/r_h, h/r_h)$. The accuracy of the equation improves as the scaled interval $\delta x/r_h$ gets smaller.
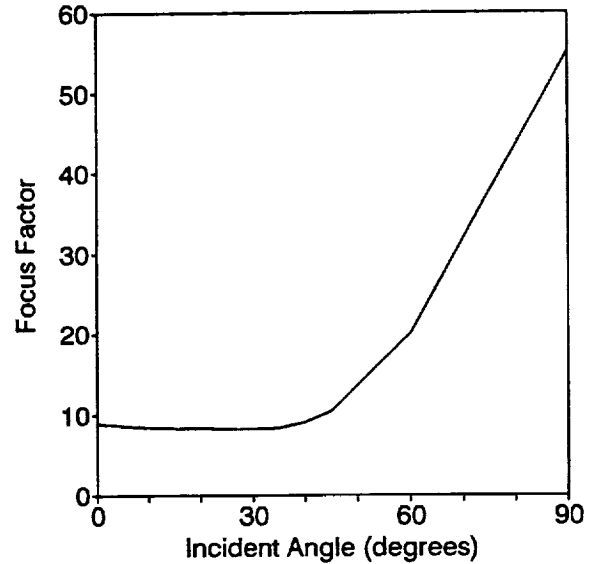
Figure 4: Focus Factor for a 3 mm radius hole as a function of angle under Low Earth Orbit (LEO) conditions as described in the text.

RESULTS

Normalized results of the computer model are tabulated in the Appendix. The tables show the focus factor as a function of the four variables; S', Θ', E', and Φ. S' is the plasma sheath thickness divided by the hole radius. Θ', is the plasma ion temperature in eV divided by the absolute value of the hole bias in Volts. E', is the directed incident kinetic energy of the ions in eV

divided by the absolute value of the hole bias in volts. Finally, Φ, is the angle between the hole's axis of symmetry and the incident velocity vector, ignoring temperature. (Φ is a characteristic of the population of ions, whereas φ is a characteristic of individual ions.)

Focus factors for low energies and high angles of incidence should be treated with caution. For low energies focus factors tend to be high. It appears that all particles entering the grid with zero velocity are collected by the hole, giving an infinite focus factor contribution. In this case the electric field due to the thermal sheath must be included to bound the focus factor. In the tables presented here focus factors in this case are bounded by the size of the calculation space instead.

Figure 5: Effect of a thermal distribution on average velocity of incident ions as the ratio, K_{zo}/qT_i varies. The velocity is normalized by the factor $\sqrt{m/2qT_i}$.

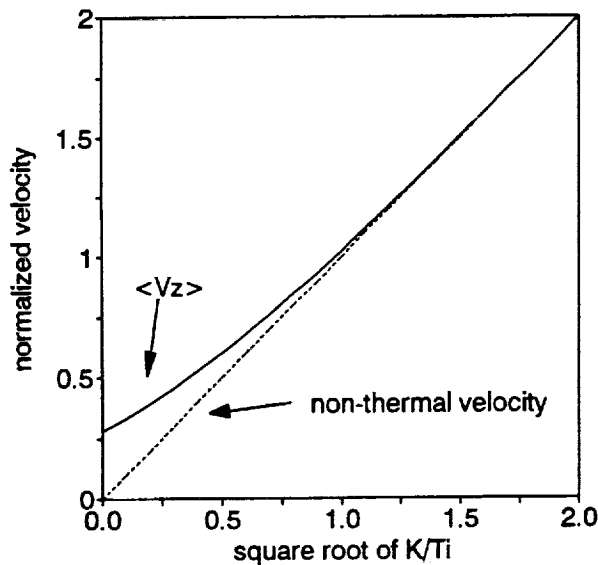At large angles of incidence there is also a possibility that the focus factors are artificially high. In this case particles which hit the hole come from far away and receive an area weighting proportional to $1/r$. However, nearby particles with a slightly different v_θ component may not be collected due to higher angular momentum. In this case the coarse sector divisions used may result in undue weight given to the large focus factor.

These tables can be interpolated for specific situations. As a example, Fig. 4 shows the focus

factor as a function of incident angle, Φ, for a 3 mm radius hole biased to -80 V in a typical low earth orbit plasma. This oxygen ion plasma has a temperature of 0.1 eV, a density of $1 \times 10^6 \text{cm}^{-3}$, and an incident kinetic energy of 4.5 eV. In this case the plasma sheath is found to be 19 mm thick so $S' = 6.4$, $\Theta' = 0.0013$, and $E' = 0.056$. A polynomial interpolation scheme[9] was used to interpolate the ram energy and angle of incidence, and a cubic spline[9] was used to interpolate the temperature and sheath thickness parameters. The ability of the of the interpolation scheme to reproduce calculated results not included in the tables is within 2%.

The focus factors from Fig. 4 show a slight decrease as the incident angle increases from zero, then a pronounced increase at higher angles of incidence. The initial decrease with angle may be due to the added angular momentum preventing particles from hitting the hole. At high angles of incidence the particles are coming from farther away. The increased area weight results in an enhanced focus factor.
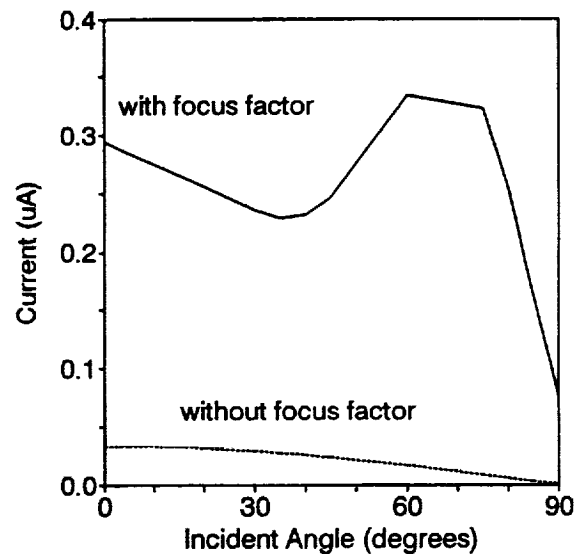
Figure 6: Ion currents to a 3 mm radius hole as a function of angle under LEO conditions, illustrating effects of the ion focusing shown in Fig. 4.

The focus factor, f, is converted into a current per hole, i, using $i = n_e q \langle v_z \rangle f A$, where A is the area of the conductive hole, n_e is the plasma density, q is the charge and $\langle v_z \rangle$ is the average ion velocity normal to the surface obtained from:

$$\langle v_z \rangle = \sqrt{\frac{2m}{qT_i\pi}} \int_0^\infty v_z e^{\frac{-m(v_z-v_{z0})^2}{2qT_i}} dv_z$$

6
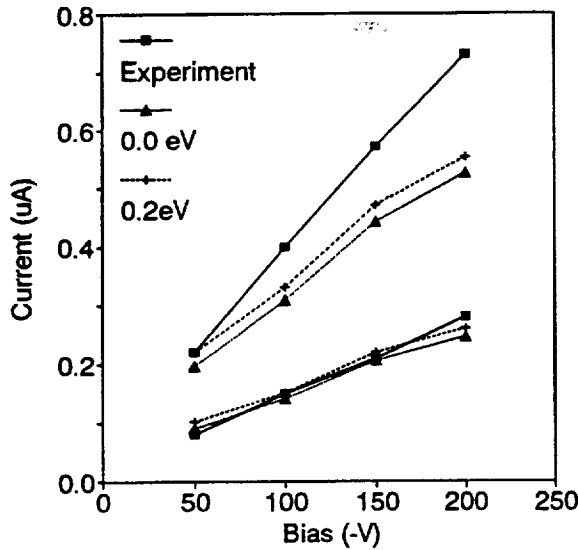
Figure 7: Comparison between Estimated Currents and Measured pinhole ion currents. The upper set of curves are obtained for a radius of 2.4 mm and the lower set is for a radius of 1.4 mm. The plasma conditions are described in the text.

or,

$$\langle v_z \rangle = \frac{1}{2}\sqrt{\frac{2qT_i}{m}} \left[\frac{e^{\frac{-K_{z0}}{qT_i}}}{\sqrt{\pi}} + \sqrt{\frac{K_{z0}}{qT_i}}\left(1 + erf\left(\sqrt{\frac{K_{z0}}{qT_i}}\right)\right)\right]$$

were v_{z0} is the initial non-thermal velocity normal to the surface, K_{z0} is the kinetic energy due to that motion and qT_i is the ion thermal energy when T_i is the ion temperature in eV. Fig. 5 shows that $\langle v_z \rangle$ converges to $\sqrt{2K_{z0}/m}$ very quickly. Assuming $\langle v_z \rangle = \sqrt{2K_{z0}/m}$ at $\sqrt{K_{z0}/qT_i} = 1$ is low by only 2.5%. Figure 6 includes the current densities to give currents to the 3 mm radius hole. In this case the current stays near 0.3 μA until very high angles of incidence where it drops off.

COMPARISON TO EXPERIMENT

The model has been compared with recent experiment measurements and is reasonably consistent with those results. However, the experiment tests only normal incidence to the hole, and does not verify the angular dependence.

Vaughn[10] has measured ion currents as a function of bias voltage to two differently sized holes. He measured the current to a 2.7 mm radius hole

and a 1.4 mm radius hole biased at from 0 V to -230 V. The Argon plasma he used had an electron temperature of 1.2 eV and an ion energy of 2.0 eV. However, the ions were thought to be cold. The number density differed between the two sets of data. For the 2.7 mm hole the density was 2×10^{12} m^{-3} giving an estimated current density of 1 mA/m^2, and for the 1.4 mm hole the density was 3×10^{12} m^{-3} giving a current density of 1.5 mA/m^2. Figure 7 compares the measured currents to those obtained from the calculated focus factor and current density. The estimated currents are shown for two cases, one with cold ions, $T_i = 0$ eV, and the other for warmer ions, $T_i = 0.2$ eV. Even for the cold case agreement is within 30% of the measured values over the -50 V to -200 V range, within the uncertainty of the plasma parameters. However, assuming warmer ions improves the agreement slightly.

CONCLUSION

The objective of this work is to produce a model which can be used to predict ion currents to insulator defects under ionospheric conditions. These currents are needed to estimate either spacecraft floating potentials or material sputter rates.

The simple approximations used in the development of the computer model described here are adequate to estimate ion currents to conductive defects on insulation. While the original intention for model development was to produce a model easily run on small computers, the addition of thermal distributions requires long computation times. However, the model has been reduced to depend on four parameters which can be tabulated. The Appendix contains tables which span a reasonable space for small holes in ionospheric conditions. These tables predict ion currents that are consistent with those measured during an initial test by other workers.

This paper only addresses part of the issue, the part dealing with individual defects geometries. In order to estimate currents and sputter rates of spacecraft surfaces, estimates of the material specific defect populations as well as estimates of the sputter yield are also needed.

REFERENCES

1. Ferguson, D. C., Snyder, D. B., Carruth, R., "Findings of the Joint Workshop on Evaluation of Impacts of Space Station Freedom Ground Configurations," NASA TM-103717, 1990.

2. Stevens, N. J., Berkopec, F. D., Purvis, C. K., Grier, N., and Staskus, J., "Investigation of high voltage spacecraft interactions with plasma environments," AIAA/DGLR 13th International Electric Propulsion Conference Paper 78-672 (1978).

3. Gabriel, S. B., Garner, C. E. and Kitamura, S., "Experimental Measurements of the Plasma Sheath Around Pinhole Defects in a Simulated High-Voltage Solar Array," AIAA Paper 83-0311 (1983).

4. Chaky, R. C., Nonnast, J. H., and Enoch, J. "Numerical simulation of sheath structure and current-voltage characteristics of a conductor-dielectric in a plasma," J. Appl. Phys. 52(12), pp. 7092-7098 (1981).

5. Brandon, S. T., Rusk, R. L., Armstrong, T. P., and Enoch, J., "Self-Consistent Simulation of Plasma Interactions with Secondary-Emitting Insulators," Spacecraft Environmental Interactions Technology 1983, NASA CP 2359, pp 287-303 (1985).

6. Mandell, M. J., and Katz, I., "Surface Interactions and High- Voltage Current Collection," Spacecraft Environmental Interactions Technology 1983, NASA CP 2359, pp 305-319 (1985).

7. McKeil, G., Balmain, K. G., "Analysis of the ion spot phenomenon on beam charged dielectrics," IEEE Trans. on Nuclear Science, Vol. NS-33, No. 6, Dec. 1986, pp.1396-1401.

8. Snyder, D. B., Herr, J. L., "Ion Collection from a Plasma by a Pinhole," 5th Annual Workshop on Space Operations, Applications and Research, July 9-11, 1991, Houston, NASA CP- 3127, Vol. II, pp. 694-702.

9. Press, W. H., Flannery, B.P., Teukolsky, S. A., Vetterling, W. T., "Numerical Recipes: The Art of Scientific Computing," Cambridge University Press, 1986.

10. Vaughn, J., "Ion Focusing Test", Electrical Grounding Tiger Team Meeting, Huntsville, Al, May 14-17, 1991.

APPENDIX

The 28 tables show the focus factor as a function of the four variables; S', Θ_i', E_i', and Φ. S' is the plasma sheath thickness divided by the hole radius and ranges from 3.6 to 11.2. Θ_i' is the plasma ion temperature in eV divided by the absolute value of the hole bias in volts and ranges from 0 to 0.2. E_i' is the directed incident kinetic energy of the ions in eV divided by the absolute value of the hole bias and ranges from 0.01 to 0.10. Finally, Φ is the angle between the hole's axis of symmetry and the incident velocity vector, ignoring temperature, and ranges from 0 to 75 degrees.

Table 1. $\Phi = 0.0$ $E_i' = 0.01$

S' \ Θ_i'	0.000	0.001	0.002	0.005	0.010	0.015	0.020
3.6	13.3	13.9	14.8	15.8	15.3	12.7	12.4
4.1	15.1	15.8	16.9	17.9	17.2	14.1	13.8
4.9	17.9	18.8	20.2	21.4	20.3	16.4	16.0
6.4	22.1	23.1	24.8	26.5	24.6	19.5	19.0
11.2	31.9	34.2	36.8	37.2	34.8	25.2	23.8

Table 2. $\Phi = 0.0$ $E_i' = 0.02$

S' \ Θ_i'	0.000	0.001	0.002	0.005	0.010	0.015	0.020
3.6	9.4	9.7	10.0	11.0	11.5	10.7	11.0
4.1	10.9	10.8	11.2	12.3	12.8	11.9	12.1
4.9	12.5	12.6	13.0	14.4	14.8	13.6	13.9
6.4	14.2	14.9	15.5	17.1	17.5	15.8	16.3
11.2	20.0	20.2	20.9	22.9	21.8	19.0	19.7

Table 3. $\Phi = 0.0$ $E_i' = 0.03$

S' \ Θ_i'	0.000	0.001	0.002	0.005	0.010	0.015	0.020
3.6	8.0	7.8	8.0	8.6	9.3	9.4	9.8
4.1	8.7	8.6	8.8	9.5	10.3	10.3	10.8
4.9	9.4	9.9	10.1	10.9	11.7	11.8	12.3
6.4	10.9	11.4	11.7	12.7	13.6	13.5	14.3
11.2	14.2	14.7	15.0	16.2	16.9	17.3	17.9

Table 4. $\Phi = 0.0$ $E_i' = 0.10$

S' \ Θ_i'	0.000	0.001	0.002	0.005	0.010	0.015	0.020
3.6	4.0	4.0	4.0	4.1	4.2	4.4	4.6
4.1	4.0	4.2	4.2	4.3	4.5	4.7	4.9
4.9	4.5	4.6	4.6	4.7	4.9	5.1	5.4
6.4	5.0	5.0	5.0	5.1	5.3	5.6	5.8
11.2	5.5	5.6	5.6	5.7	6.0	6.1	6.5

Table 5. $\Phi = 5.0$ $E'_i = 0.01$

S' Θ'_i	0.000	0.001	0.002	0.005	0.010	0.015	0.020
3.6	13.1	13.8	14.6	15.2	14.6	12.1	11.8
4.1	14.9	15.6	16.5	17.2	16.4	13.5	13.2
4.9	18.0	18.6	19.6	20.3	19.3	15.7	15.5
6.4	21.8	22.6	23.8	24.5	23.3	18.4	18.5
11.2	32.4	32.2	33.4	32.0	27.0	20.0	17.9

Table 6. $\Phi = 5.0$ $E'_i = 0.02$

S' Θ'_i	0.000	0.001	0.002	0.005	0.010	0.015	0.020
3.6	9.6	9.7	9.9	10.7	10.9	10.1	10.3
4.1	10.4	10.7	11.0	11.9	12.1	11.1	11.4
4.9	12.5	12.4	12.7	13.7	13.8	12.7	13.1
6.4	14.6	14.6	14.9	15.9	15.9	14.3	14.8
11.2	19.6	18.9	18.9	19.4	17.6	14.8	14.2

Table 7. $\Phi = 5.0$ $E'_i = 0.03$

S' Θ'_i	0.000	0.001	0.002	0.005	0.010	0.015	0.020
3.6	7.7	7.8	7.9	8.4	8.8	8.8	9.1
4.1	8.4	8.5	8.7	9.2	9.7	9.6	9.9
4.9	9.5	9.7	9.8	10.4	10.9	10.8	11.1
6.4	11.2	11.2	11.3	11.8	12.2	11.9	12.1
11.2	14.3	13.6	13.5	13.7	13.1	12.3	11.5

Table 8. $\Phi = 5.0$ $E'_i = 0.10$

S' Θ'_i	0.000	0.001	0.002	0.005	0.010	0.015	0.020
3.6	3.9	3.9	3.9	4.0	4.1	4.2	4.3
4.1	4.2	4.2	4.2	4.2	4.3	4.4	4.5
4.9	4.5	4.5	4.5	4.5	4.5	4.6	4.7
6.4	5.0	4.8	4.7	4.7	4.7	4.8	4.8
11.2	5.7	5.0	4.7	4.5	4.5	4.3	4.2

Table 9. $\Phi = 15.0$ $E'_i = 0.01$

S' Θ'_i	0.000	0.001	0.002	0.005	0.010	0.015	0.020
3.6	13.6	14.0	14.5	14.5	13.4	11.1	10.8
4.1	15.5	15.8	16.3	16.2	14.8	12.2	11.7
4.9	18.3	18.5	19.0	18.6	16.8	13.6	12.8
6.4	22.7	22.1	22.4	22.2	18.8	14.6	13.7
11.2	33.3	29.0	27.7	22.8	17.9	13.2	11.9

Table 10. $\Phi = 15.0$ $E'_i = 0.02$

S' Θ'_i	0.000	0.001	0.002	0.005	0.010	0.015	0.020
3.6	10.0	9.8	9.9	10.3	10.0	9.1	9.0
4.1	11.0	10.8	10.9	11.2	10.8	9.8	9.5
4.9	12.8	12.4	12.4	12.6	11.9	10.5	10.3
6.4	15.0	14.3	14.1	13.9	12.7	11.0	10.8
11.2	20.5	16.6	15.4	13.5	11.1	9.1	8.9

Table 11. $\Phi = 15.0$ $E'_i = 0.03$

S' Θ'_i	0.000	0.001	0.002	0.005	0.010	0.015	0.020
3.6	7.9	7.9	7.9	8.1	8.1	7.8	7.1
4.1	8.8	8.6	8.6	8.8	8.7	8.3	7.4
4.9	9.9	9.7	9.6	9.6	9.3	8.8	7.7
6.4	11.9	10.9	10.7	10.3	9.7	9.0	7.7
11.2	15.0	11.8	10.8	9.3	7.9	7.4	6.2

Table 12. $\Phi = 15.0$ $E'_i = 0.10$

S' Θ'_i	0.000	0.001	0.002	0.005	0.010	0.015	0.020
3.6	4.1	4.0	3.9	3.9	3.8	3.8	3.7
4.1	4.3	4.2	4.1	4.0	3.9	3.8	3.8
4.9	4.8	4.4	4.3	4.1	3.9	3.7	3.7
6.4	5.2	4.5	4.3	3.9	3.6	3.4	3.3
11.2	5.8	3.9	3.5	3.0	2.6	2.3	2.3

Table 13. $\Phi = 30.0$ $E'_i = 0.01$

S' Θ'_i	0.000	0.001	0.002	0.005	0.010	0.015	0.020
3.6	15.5	15.2	15.2	14.1	10.6	9.8	7.3
4.1	17.6	16.9	16.8	15.4	11.3	10.4	7.7
4.9	20.8	19.4	19.2	17.2	12.2	11.2	7.9
6.4	25.3	22.7	21.9	19.2	12.8	12.0	8.0
11.2	37.2	26.4	22.8	17.0	10.5	9.7	6.2

Table 14. $\Phi = 30.0$ $E'_i = 0.02$

S' Θ'_i	0.000	0.001	0.002	0.005	0.010	0.015	0.020
3.6	11.2	10.6	10.5	10.1	9.2	8.0	6.6
4.1	12.4	11.6	11.4	10.9	9.7	8.4	6.8
4.9	14.4	13.1	12.7	11.7	10.3	8.8	6.9
6.4	17.0	14.6	13.8	12.2	10.7	9.1	6.8
11.2	23.0	15.1	13.4	10.5	8.2	7.6	5.0

Table 15. $\Phi = 30.0$ $E'_i = 0.03$

S' Θ'_i	0.000	0.001	0.002	0.005	0.010	0.015	0.020
3.6	9.1	8.5	8.4	8.2	7.7	7.0	6.1
4.1	10.2	9.3	9.0	8.7	8.0	7.2	6.2
4.9	11.5	10.2	9.8	9.2	8.3	7.3	6.3
6.4	12.9	11.1	10.3	9.2	8.1	7.3	6.1
11.2	15.5	11.2	10.2	8.2	6.5	5.9	4.9

Table 16. $\Phi = 30.0$ $E'_i = 0.10$

S' Θ'_i	0.000	0.001	0.002	0.005	0.010	0.015	0.020
3.6	4.7	4.3	4.1	3.9	3.6	3.4	3.3
4.1	4.9	4.4	4.2	3.8	3.5	3.3	3.2
4.9	5.3	4.5	4.2	3.7	3.4	3.2	3.0
6.4	5.4	4.1	4.0	3.7	3.3	3.1	2.9
11.2	7.2	6.9	6.3	5.0	3.9	3.4	3.1

Table 17. $\Phi = 45.0$ $E_i' = 0.01$

S' Θ_i'	0.000	0.001	0.002	0.005	0.010	0.015	0.020
3.6	19.3	17.8	16.8	13.7	10.4	7.5	6.9
4.1	21.4	19.7	18.8	15.0	11.1	7.9	7.1
4.9	25.1	22.7	21.7	16.7	12.0	8.2	7.5
6.4	30.6	26.1	24.6	18.4	13.0	8.3	7.8
11.2	45.6	31.9	25.4	15.7	11.2	7.2	6.0

Table 18. $\Phi = 45.0$ $E_i' = 0.02$

S' Θ_i'	0.000	0.001	0.002	0.005	0.010	0.015	0.020
3.6	13.5	12.4	12.2	10.8	8.8	6.9	6.2
4.1	14.9	13.6	13.3	11.6	9.2	7.1	6.5
4.9	17.6	15.3	14.8	12.5	9.8	7.4	6.9
6.4	20.4	17.0	15.9	13.2	8.7	7.6	7.4
11.2	26.9	23.6	19.5	12.7	9.2	6.7	6.1

Table 19. $\Phi = 45.0$ $E_i' = 0.03$

S' Θ_i'	0.000	0.001	0.002	0.005	0.010	0.015	0.020
3.6	10.9	10.0	9.8	9.1	7.8	6.5	5.2
4.1	12.3	10.9	10.6	9.6	8.1	6.6	5.3
4.9	13.9	11.9	11.4	10.2	8.5	6.9	5.4
6.4	15.9	12.8	12.3	10.8	8.9	7.3	5.5
11.2	23.4	20.2	16.9	11.4	8.3	6.9	5.1

Table 20. $\Phi = 45.0$ $E_i' = 0.10$

S' Θ_i'	0.000	0.001	0.002	0.005	0.010	0.015	0.020
3.6	5.6	5.0	4.7	4.4	4.2	4.0	3.6
4.1	5.7	4.7	4.7	4.6	4.4	4.1	3.7
4.9	5.6	5.5	5.6	5.4	4.9	4.4	4.0
6.4	7.6	7.4	7.3	6.5	5.5	4.9	4.4
11.2	13.8	12.6	10.8	7.9	5.9	5.2	4.4

Table 21. $\Phi = 60.0$ $E_i' = 0.01$

S' Θ_i'	0.000	0.001	0.002	0.005	0.010	0.015	0.020
3.6	25.8	22.4	18.7	13.5	9.0	7.6	6.2
4.1	28.5	26.0	21.4	15.0	9.5	8.0	6.3
4.9	34.4	31.8	25.8	18.5	10.4	8.7	7.1
6.4	43.4	39.5	31.0	19.4	11.3	9.7	7.8
11.2	75.1	46.3	29.6	17.0	10.4	8.3	5.8

Table 22. $\Phi = 60.0$ $E_i' = 0.02$

S' Θ_i'	0.000	0.001	0.002	0.005	0.010	0.015	0.020
3.6	18.1	17.4	16.1	12.2	8.6	6.0	5.3
4.1	20.6	19.8	18.3	13.6	9.1	6.2	5.4
4.9	25.0	23.5	21.8	15.3	10.0	6.5	5.9
6.4	30.6	28.9	25.8	17.2	11.0	7.3	6.6
11.2	60.5	36.2	24.9	15.5	8.9	6.3	5.5

Table 23. $\Phi = 60.0$ $E_i' = 0.03$

S' Θ_i'	0.000	0.001	0.002	0.005	0.010	0.015	0.020
3.6	15.4	14.5	13.9	11.3	7.6	6.3	4.5
4.1	17.1	16.3	15.6	12.6	8.0	6.6	4.7
4.9	20.2	19.1	18.5	14.1	8.7	7.4	5.0
6.4	24.4	24.8	22.5	15.9	9.8	8.2	5.6
11.2	51.0	31.2	21.7	13.7	8.9	7.2	5.1

Table 24. $\Phi = 60.0$ $E_i' = 0.10$

S' Θ_i'	0.000	0.001	0.002	0.005	0.010	0.015	0.020
3.6	7.8	8.1	8.3	8.0	6.6	5.4	4.5
4.1	9.5	9.7	9.8	9.1	7.2	5.8	4.8
4.9	12.2	12.3	12.0	10.2	7.7	6.3	5.3
6.4	16.2	15.6	14.1	10.8	8.0	6.5	5.3
11.2	29.7	20.4	15.5	10.1	7.6	6.3	5.0

Table 25. $\Phi = 75.0$ $E_i' = 0.01$

S' Θ_i'	0.000	0.001	0.002	0.005	0.010	0.015	0.020
3.6	40.2	24.6	17.8	12.9	7.5	6.1	5.3
4.1	55.5	30.5	21.1	14.6	8.0	6.5	5.6
4.9	76.6	40.9	26.9	17.0	8.8	7.1	6.1
6.4	108.	55.8	32.9	20.2	9.9	7.7	6.8
11.2	211.	44.2	26.4	15.8	8.1	6.6	5.2

Table 26. $\Phi = 75.0$ $E_i' = 0.02$

S' Θ_i'	0.000	0.001	0.002	0.005	0.010	0.015	0.020
3.6	34.4	24.1	18.7	11.6	8.2	5.1	4.4
4.1	48.1	30.4	22.7	13.4	8.9	5.4	4.6
4.9	64.1	41.6	29.7	15.3	10.1	6.0	5.1
6.4	92.4	51.6	34.9	17.1	11.2	6.9	5.8
11.2	160.	28.6	20.1	12.8	9.7	5.8	4.9

Table 27. $\Phi = 75.0$ $E_i' = 0.03$

S' Θ_i'	0.000	0.001	0.002	0.005	0.010	0.015	0.020
3.6	31.4	23.8	19.3	10.9	7.8	6.0	4.0
4.1	43.6	30.4	23.8	12.7	8.3	6.5	4.3
4.9	57.6	42.1	30.7	14.6	9.3	7.5	4.8
6.4	92.4	49.8	32.1	16.3	10.4	8.6	5.4
11.2	132.	22.7	16.6	11.3	7.6	6.6	4.5

Table 28. $\Phi = 75.0$ $E_i' = 0.10$

S' Θ_i'	0.000	0.001	0.002	0.005	0.010	0.015	0.020
3.6	27.3	21.7	17.7	11.3	7.6	5.7	4.4
4.1	32.7	26.0	20.0	11.9	7.8	5.9	4.6
4.9	40.4	29.4	21.2	12.1	7.8	6.1	5.1
6.4	51.6	29.9	20.3	10.9	7.5	6.7	5.5
11.2	84.4	16.7	10.8	7.8	6.1	5.2	4.3

REPORT DOCUMENTATION PAGE

1. AGENCY USE ONLY (Leave blank)	2. REPORT DATE	3. REPORT TYPE AND DATES COVERED
	April 1993	Technical Memorandum

4. TITLE AND SUBTITLE

Plasma Sheath Effects on Ion Collection by a Pinhole

5. FUNDING NUMBERS

WU–506–41–41

6. AUTHOR(S)

Joel L. Herr and David B. Snyder

7. PERFORMING ORGANIZATION NAME(S) AND ADDRESS(ES)

National Aeronautics and Space Administration
Lewis Research Center
Cleveland, Ohio 44135–3191

8. PERFORMING ORGANIZATION REPORT NUMBER

E–7740

9. SPONSORING/MONITORING AGENCY NAMES(S) AND ADDRESS(ES)

National Aeronautics and Space Administration
Washington, D.C. 20546–0001

10. SPONSORING/MONITORING AGENCY REPORT NUMBER

NASA TM–106098

12a. DISTRIBUTION/AVAILABILITY STATEMENT

Unclassified - Unlimited
Subject Category 18

12b. DISTRIBUTION CODE

13. ABSTRACT (Maximum 200 words)

This work presents tables to assist in the evaluation of pinhole collection effects on spacecraft. These tables summarize results of a computer model which tracks particle trajectories through a simplified electric field in the plasma sheath. A technique is proposed to account for plasma sheath effects in the application of these results and scaling rules are proposed to apply the calculations to specific situations. This model is compared to ion current measurements obtained by another worker, and the agreement is very good.

14. SUBJECT TERMS

Ion current collection; Focus factors; Sputtering

15. NUMBER OF PAGES
12

16. PRICE CODE
A03

17. SECURITY CLASSIFICATION OF REPORT	18. SECURITY CLASSIFICATION OF THIS PAGE	19. SECURITY CLASSIFICATION OF ABSTRACT	20. LIMITATION OF ABSTRACT
Unclassified	Unclassified	Unclassified	